

# Three-level ion optical clocks

C. A. Holliman,\* M. Fan, and A. M. Jayich

*Department of Physics, University of California, Santa Barbara, California 93106, USA*

(Dated: November 11, 2022)

To reduce complexity and increase system robustness we propose an optical clock with trapped alkaline-earth-like ions that use only three electronic states for clock operation. Compared to traditional single ion clocks this reduces the number of lasers required. The proposed clock uses hyperfine levels for clock readout operations and therefore requires nuclear spin  $I > 0$ . The primary limitation for such a clock is due to state detection errors from off-resonant scattering events. In general, large hyperfine splittings reduce state detection errors, making systems with large nuclei appealing for realizing a three-level clock. We consider the  $^{225}\text{Ra}^+$  ion as a candidate system for a three-level clock, and discuss the potential to help realize a transportable optical clock.

## I. INTRODUCTION

Transportable optical clocks are promising for tests of Einstein's equivalence principle [1], searches for dark matter [2], and improved timekeeping and global positioning systems [3]. In combination with clock networks on Earth, optical clocks on satellites would improve limits on the accuracy of intercontinental frequency transfer and comparison, and aid deep space navigation [4, 5]. However, there is a gap between existing state-of-the-art optical clocks and the desired turn-key systems that can be deployed, or even run autonomously, e.g. as part of an advanced global positioning system network. Generation, control, and delivery of laser light with integrated photonics is desirable for such advanced clocks. The use of integrated photonics is promising for achieving smaller clock form factors and system robustness, where optical alignment can be lithographically defined. We propose optical clock systems that operate with three or even two lasers, with wavelengths longer than 400 nm. Both features should reduce the barriers for realizing a clock with integrated photonics.

Clocks based on trapped ions that can be directly laser cooled are a potential path towards robust transportable optical clocks. Ion traps use electromagnetic potentials which result in long storage times, and clock operation only needs low-power lasers. In realizations with candidate systems  $\text{Ca}^+$  and  $\text{Sr}^+$  [6, 7], the excited clock state is separate from the states used for laser cooling and state detection, and an additional laser is needed to reset the electronic population between clock interrogations [8, 9]. In total, five electronic states are used along with four laser wavelengths for these relatively simple clocks. To further ease requirements for the use of integrated photonics, the number of required lasers can be reduced from four to three, or possibly only two lasers with optical clocks based on three-level  $\Lambda$  systems.

Alkaline-earth-like ions with nuclear spin  $I > 0$  can realize clock operation in a three-level  $\Lambda$  system by using their hyperfine structure. In the proposed scheme only

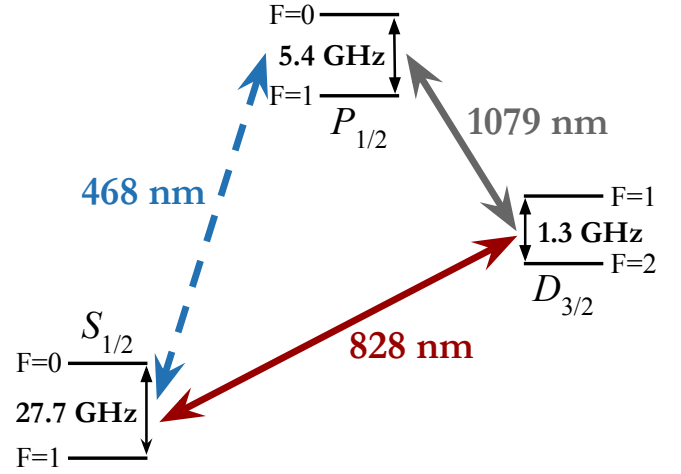


FIG. 1. The  $^{225}\text{Ra}^+$  level structure for clock operation showing the Doppler cooling (blue), repump (gray), and clock (red) transitions. Hyperfine splittings of the states are shown. For two-laser clock operation, the 468 nm laser is not required.

three electronic transitions are driven: the  $S_{1/2} \rightarrow D_{3/2}$  clock transition, the  $S_{1/2} \rightarrow P_{1/2}$  Doppler cooling transition, and the  $D_{3/2} \rightarrow P_{1/2}$  repump transition, see the levels in our example system Fig. 1. Similar to the  $^{171}\text{Yb}^+$  [26] and  $^{199}\text{Hg}^+$  [27] clocks, alkaline-earth-like ions with nuclear spin  $I > 0$  have magnetic field insensitive clock transitions and can be directly laser cooled [28–30]. The  $\text{Yb}^+$  ion (E2) clock operates on the  $S_{1/2} \rightarrow D_{3/2}$  transition ( $\lambda = 435.5$  nm) in a four-level system, where repumping to the  $[3/2]_{3/2}$  state is done with light at 935 nm [22]. Background gas collisions can also populate the  $\text{Yb}^+$  ion's very long-lived  $F_{7/2}$  state. This population can be pumped back into the laser cooling states with an additional laser [31], or a new  $\text{Yb}^+$  ion can be loaded into the trap. For the  $\text{Yb}^+$  ion, state detection, which determines if the clock transition was driven, relies on detecting population in distinct hyperfine levels due to the interconnectedness of the electronic  $\Lambda$  structure [21]. Off-resonant scattering limits the state detection fidelity, and we calculate these state detection errors for candidate clock ions. Larger hyperfine splittings result in lower

\* cholliman3@gmail.com

TABLE I. Relevant atomic properties for alkaline-earth-like ions are given, including the  $S_{1/2} \rightarrow P_{1/2}$  transition linewidth,  $P_{1/2}$  state to  $S_{1/2}$  state branching fraction  $p$ , transition wavelengths (nm), differential scalar polarizability  $\alpha_0$  (atomic units) of the  $S_{1/2} \rightarrow D_{3/2}$  clock transition, and  $D_{3/2}$  state lifetime.

Ion	$\Gamma/2\pi$ (MHz)	$p$	$\lambda_{\text{cool}}$	$\lambda_{\text{repump}}$	$\lambda_{\text{clock}}$	$\alpha_0$	$\tau_{3/2}$ (s)
Ca <sup>+</sup>	22.4 [10]	0.93565 [11]	397	866	732	-44.1(6) [12]	1.176(11) [13]
Sr <sup>+</sup>	21.5 [14]	0.94498 [15]	422	1092	687	-26.9(1.1) [16]	0.435(4) [17]
Ba <sup>+</sup>	20.3 [18]	0.73182 [18]	493	650	2052	-75.4(1.1) [16]	79.8(4.6) [19]
Yb <sup>+</sup>	19.6 [20]	0.995 [21]	369.5	2438	435.5	-42(8) [22]	0.052(1) [23]
Ra <sup>+</sup>	18.3 [24]	0.9104 [25]	468	1079	828	-20.8(1.7) [16]	0.638(10) [24]

state detection errors due to off-resonant scattering. For species with large hyperfine splittings, generally heavy atoms, the clock performance is not limited by state detection errors. Here we extend work with hyperfine ion clocks to alkaline-earth-like ion systems with  $I > 0$ , see Table I, that can realize three-level operation and have wavelengths farther from the UV when compared to the Yb<sup>+</sup> ion, which requires Doppler cooling light at 369.5 nm. We consider such a heavy ion, <sup>225</sup>Ra<sup>+</sup>, as an example system for a three-level clock, and discuss its potential to realize a transportable clock.

## II. THREE-LASER CLOCK OPERATION

Four steps constitute a three-level ion optical clock measurement sequence: laser cooling, state preparation, clock interrogation, and state detection, see Fig. 2. Driving the  $S_{1/2} \rightarrow P_{1/2}$  and  $D_{3/2} \rightarrow P_{1/2}$  transitions laser cools the ion. The population is then prepared to a  $|S_{1/2}, F, m = 0\rangle$  sublevel in the  $S_{1/2}$  ground state, where  $F$  denotes the hyperfine level and  $m$  denotes the magnetic sublevel. The  $S_{1/2} \rightarrow D_{3/2}$  clock transition is then interrogated with either a Rabi or Ramsey measurement [32]. During state detection, scattered  $S_{1/2} \rightarrow P_{1/2}$  photons are collected onto a detector. If the total photon counts exceeds a predetermined detection threshold, the state detection event is characterized as “bright”, otherwise the event is characterized as “dark”. These bright and dark state detection events determine the probability that the clock transition was driven.

In the following subsections we consider a <sup>225</sup>Ra<sup>+</sup> clock, nuclear spin  $I = 1/2$ , and describe operation for two different clock protocols: one requires a microwave source, and another requires Doppler cooling light polarized to drive  $\pi$  transitions. For nuclear spin  $I > 1/2$ , we consider a <sup>137</sup>Ba<sup>+</sup> clock, nuclear spin  $I = 3/2$ , and describe clock operation with Doppler cooling light polarized to drive  $\pi$  transitions.

### A. Microwave sequence, $I = 1/2$

In the first sequence described a microwave source and addressing three electronic transitions is required, see

Fig. 2. Driving the  $|S_{1/2}, F = 0\rangle \rightarrow |P_{1/2}, F = 1\rangle$  and  $|S_{1/2}, F = 1\rangle \rightarrow |P_{1/2}, F = 1\rangle$  transitions Doppler cools the ion. Any decays to the  $D_{3/2}$  state are repumped to the  $P_{1/2}$  state by driving the  $|D_{3/2}, F = 1\rangle \rightarrow |P_{1/2}, F = 1\rangle$  and  $|D_{3/2}, F = 2\rangle \rightarrow |P_{1/2}, F = 1\rangle$  transitions. The population is then prepared in the  $|S_{1/2}, F = 0, m = 0\rangle$  state by turning off the light driving the  $|S_{1/2}, F = 0\rangle \rightarrow |P_{1/2}, F = 1\rangle$  transition [27]. The  $|S_{1/2}, F = 0, m = 0\rangle \rightarrow |D_{3/2}, F = 2, m = 0\rangle$  electric quadrupole transition is probed followed by a  $|D_{3/2}, F = 2, m = 0\rangle \rightarrow |D_{3/2}, F = 1, m = 0\rangle$  microwave  $\pi$ -pulse at 1.3 GHz. The  $|S_{1/2}, F = 1\rangle \rightarrow |P_{1/2}, F = 0\rangle$  and  $|D_{3/2}, F = 1\rangle \rightarrow |P_{1/2}, F = 0\rangle$  transitions are then used for state detection of the population. If the ion remains in the  $|S_{1/2}, F = 0\rangle$  state, the resulting state detection event is dark. Otherwise, if the clock interrogation drives the ion to the  $|D_{3/2}, F = 2\rangle$ , it is subsequently shelved to the  $|D_{3/2}, F = 1\rangle$  state with the microwave pulse and the state detection event is bright.

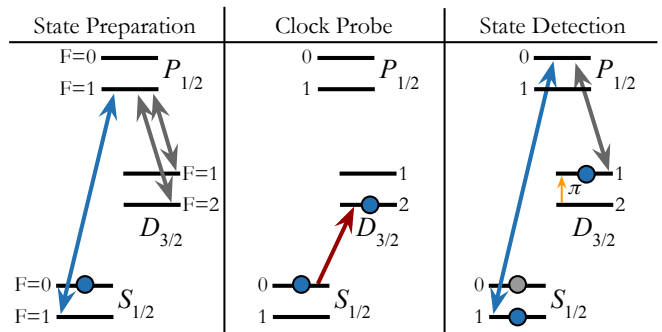


FIG. 2. The microwave clock measurement sequence for a <sup>225</sup>Ra<sup>+</sup> ion optical clock based on the  $S_{1/2} \rightarrow D_{3/2}$  transition (red). The total angular momentum quantum number  $F$  is shown next to each level. Arrows represent transitions between hyperfine levels, blue circles represent populated hyperfine levels, and gray circles represent the dark state during state detection. The  $S_{1/2} \rightarrow P_{1/2}$  Doppler cooling transition (blue),  $D_{3/2} \rightarrow P_{1/2}$  repump transition (gray), and  $|D_{3/2}, F = 2, m = 0\rangle \rightarrow |D_{3/2}, F = 1, m = 0\rangle$  microwave transition (yellow) are shown.

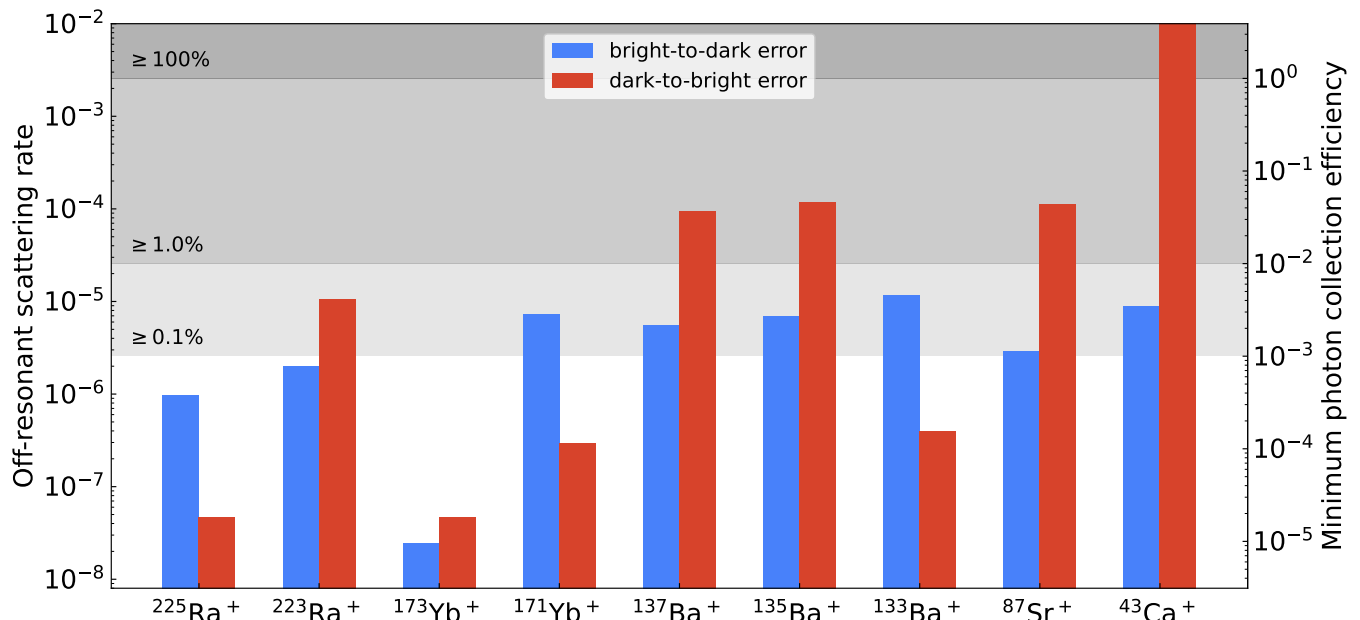


FIG. 3. Bright-to-dark (blue) and dark-to-bright (red) state detection errors for alkaline-earth-like three-level ion optical clocks. The left y-axis shows the off-resonant scattering rates, and the right y-axis shows the minimum photon collection efficiency needed for a 95% state detection fidelity with the requirement that 20 photons are collected on average when the ion is in a bright state. Gray shadings show the 100%, 1%, and 0.1% collection efficiency cutoffs. A collection efficiency above 100% is not possible as it would require counting more photons than emitted by the ion.

### B. Polarization sequence, $I = 1/2$

The polarization clock sequence requires driving three electronic transitions and using Doppler cooling light polarized to drive  $\pi$  transitions. Laser cooling uses the same transitions as in the microwave sequence: the  $|S_{1/2}, F = 0\rangle \rightarrow |P_{1/2}, F = 1\rangle$ ,  $|S_{1/2}, F = 1\rangle \rightarrow |P_{1/2}, F = 1\rangle$ ,  $|D_{3/2}, F = 1\rangle \rightarrow |P_{1/2}, F = 1\rangle$ , and  $|D_{3/2}, F = 2\rangle \rightarrow |P_{1/2}, F = 1\rangle$  transitions. But, state preparation requires a magnetic field and laser polarization to drive  $|S_{1/2}, F = 1\rangle \rightarrow |P_{1/2}, F = 1\rangle$   $\pi$  transitions which prepare the population in the  $|S_{1/2}, F = 1, m = 0\rangle$  sublevel [30, 33]. The  $|S_{1/2}, F = 1, m = 0\rangle \rightarrow |D_{3/2}, F = 2, m = 0\rangle$  electric quadrupole transition is then probed. The  $|S_{1/2}, F = 1\rangle \rightarrow |P_{1/2}, F = 0\rangle$  and  $|D_{3/2}, F = 1\rangle \rightarrow |P_{1/2}, F = 0\rangle$  transitions are then used for state detection of the population. If the clock transition is driven the population will be in a dark state.

### C. Polarization sequence, $I > 1/2$

The polarization clock sequence for species with nuclear spin  $I > 1/2$  requires driving three electronic transitions and using Doppler cooling light polarized to drive  $\pi$  transitions during state preparation. For  $^{137}\text{Ba}^+$ , driving the  $|S_{1/2}, F = 2\rangle \rightarrow |P_{1/2}, F = 2\rangle$ ,  $|S_{1/2}, F = 1\rangle \rightarrow |P_{1/2}, F = 2\rangle$ , and  $|S_{1/2}, F = 2\rangle \rightarrow |P_{1/2}, F = 1\rangle$  transitions Doppler cools the ion. Decays to the  $D_{3/2}$  state are

repumped to the  $P_{1/2}$  state by driving the  $|D_{3/2}, F = 0\rangle \rightarrow |P_{1/2}, F = 1\rangle$ ,  $|D_{3/2}, F = 1\rangle \rightarrow |P_{1/2}, F = 1\rangle$ ,  $|D_{3/2}, F = 2\rangle \rightarrow |P_{1/2}, F = 1\rangle$ , and  $|D_{3/2}, F = 3\rangle \rightarrow |P_{1/2}, F = 2\rangle$  transitions. The population is then prepared in the  $|S_{1/2}, F = 1, m = 0\rangle$  state by stroboscopically driving the  $|S_{1/2}, F = 1\rangle \rightarrow |P_{1/2}, F = 1\rangle$  and  $|S_{1/2}, F = 2\rangle \rightarrow |P_{1/2}, F = 1\rangle$  transitions [33]. The  $|S_{1/2}, F = 1, m = 0\rangle \rightarrow |D_{3/2}, F = 3, m = 0\rangle$  electric quadrupole transition is probed. The same transitions for laser cooling are then used for state detection of the population with the exception of the  $|S_{1/2}, F = 1\rangle \rightarrow |P_{1/2}, F = 2\rangle$  and  $|D_{3/2}, F = 3\rangle \rightarrow |P_{1/2}, F = 2\rangle$  transitions. If the clock transition is driven the population will be in a dark state.

## III. STATE DETECTION FIDELITY

State detection requires one or more cooling lasers and one or more repump lasers to be incident at the ion. The  $S_{1/2}$  and  $D_{3/2}$  hyperfine levels that these lasers address are called the bright states, and the other levels are called dark states. The driven transitions form a closed loop with electric dipole selection rules, but off-resonant scattering could drive other transitions that either leak population out of the loop or pump population into the loop. We define a bright-to-dark error as the probability that the population is off-resonantly driven from a bright state to a dark state for each  $S_{1/2} \rightarrow P_{1/2}$  cooling photon scattered, and a dark-to-bright error as the probability that

the population is off-resonantly driven from a dark state to a bright state for each  $S_{1/2} \rightarrow P_{1/2}$  cooling photon scattered.

We make the following approximations to calculate the off-resonant scattering error. We first assume that the spectra of these dipole transitions are Lorentzians with natural linewidths, and that there is no power broadening, Doppler broadening, or Zeeman shifts. If the ion is bright, we assume that the population is in an equilibrium distribution of all bright states. The fraction of population in each of the  $S_{1/2}$  and  $D_{3/2}$  hyperfine levels is determined by the electronic and hyperfine branching fractions. If the ion is dark, we assume that the population is in a single dark state that the clock transition drives to or drives from. We also assume that there is no off-resonant scattering from a repump laser to a cooling transition or vice versa.

We can write the bright-to-dark error for each cooling transition photon scattered as

$$\epsilon_{\text{bd}} = \sum_i^{\text{b} \rightarrow \text{d driven}} \sum_j q_i q_j r_{i,\text{dark}} L(\delta_{i,j}, \Gamma) / p, \quad (1)$$

where  $\sum_i^{\text{b} \rightarrow \text{d}}$  is a summation over all electric dipole transitions from bright states,  $S_{1/2} \rightarrow P_{1/2}$  and  $D_{3/2} \rightarrow P_{1/2}$ , where the upper  $P_{1/2}$  state of the transition can branch into dark states,  $\sum_j^{\text{driven}}$  is a summation over all electric dipole transitions that are driven during the state detection,  $q_i (q_j)$  is the equilibrium population in the lower state of the  $i$  ( $j$ ) transition,  $r_{i,\text{dark}}$  is the branching fraction from the upper state of the  $i$  transition to a dark state,  $\delta_{i,j}$  is the frequency detuning between the  $i$  and  $j$  transitions,  $\Gamma$  is the decay rate of the  $P_{1/2}$  state,  $p$  is the electronic branching fraction from the  $P_{1/2}$  state to the  $S_{1/2}$  state, and  $L(\delta_{i,j}, \Gamma)$  is a Lorentzian function with the peak normalized to unity,

$$L(\delta_{i,j}, \Gamma) = \frac{1}{4\delta_{i,j}^2 / \Gamma^2 + 1}. \quad (2)$$

The dark-to-bright error for each cooling transition photon scattered is

$$\epsilon_{\text{db}} = \sum_i^{\text{d} \rightarrow \text{b driven}} \sum_j q_i q_j r_{i,\text{bright}} L(\delta_{i,j}, \Gamma) / p, \quad (3)$$

where  $\sum_i^{\text{d} \rightarrow \text{b}}$  is a summation over all electric dipole transitions from dark states where the upper state of the transition can branch into bright states, and  $r_{i,\text{bright}}$  is the branching fraction from the upper state of the  $i$  transition to a bright state.

For the microwave sequence and the example case of  $^{225}\text{Ra}^+$ , see Fig. 2, we discuss the state detection infidelities. During state detection, the  $|S_{1/2}, F = 1\rangle \rightarrow$

$|P_{1/2}, F = 0\rangle$  is driven, but off-resonant scattering results in two sources of bright-to-dark error and one source of dark-to-bright error. A bright-to-dark error can occur when the state detection light addressing the  $|S_{1/2}, F = 1\rangle \rightarrow |P_{1/2}, F = 0\rangle$  off-resonantly drives the  $|S_{1/2}, F = 1\rangle \rightarrow |P_{1/2}, F = 1\rangle$  transition, which is detuned by the  $P_{1/2}$  state hyperfine splitting (5.45 GHz). A bright-to-dark error can also occur when the state detection light addressing the  $|D_{3/2}, F = 1\rangle \rightarrow |P_{1/2}, F = 0\rangle$  transition off-resonantly drives the  $|D_{3/2}, F = 1\rangle \rightarrow |P_{1/2}, F = 1\rangle$  transition, which is also detuned by the HF<sub>P</sub> splitting. The dark-to-bright error can occur when the  $|S_{1/2}, F = 1\rangle \rightarrow |P_{1/2}, F = 0\rangle$  state detection light drives the  $|S_{1/2}, F = 0\rangle \rightarrow |P_{1/2}, F = 1\rangle$  transition. But, this transition is detuned from the laser frequency by the sum of the  $P_{1/2}$  and  $S_{1/2}$  state hyperfine splittings (5.45 and 27.7 GHz, respectively [42]). This large detuning, 33.1 GHz, makes the microwave sequence, Sec. II A, more robust to dark-to-bright errors compared to the polarization sequence where the detuning is only the  $D_{3/2}$  state hyperfine splitting (1.3 GHz [43]) Sec. II B. For the microwave sequence the probability of a bright-to-dark error is  $\epsilon_{\text{bd}} = 8.9 \times 10^{-7}$ , and  $\epsilon_{\text{db}} = 4.3 \times 10^{-8}$  for a dark-to-bright error. Errors for other non-zero nuclear spin isotopes are shown in Table II.

The off-resonant scattering rates for bright-to-dark and dark-to-bright errors, and the associated minimum photon collection efficiency needed to obtain a 95% state detection fidelity are shown in Fig. 3. The minimum photon collection efficiency is calculated with the requirement that on average 20 photons are collected during state detection. For  $I = 1/2$  isotopes, the systems are robust against dark-to-bright errors, while for  $I > 1/2$  isotopes, the four hyperfine levels in the  $D_{3/2}$  state make the systems more susceptible to dark-to-bright errors during state detection. For a 95% state detection fidelity, the  $^{225}\text{Ra}^+$  ion requires a 0.038% photon collection efficiency, considerably lower than the 0.28% photon collection efficiency demonstrated for a  $^{226}\text{Ra}^+$  ion optical clock [44]. The  $^{173}\text{Yb}^+$  ion has the lowest state detection error, 0.03%, among the ions considered. The low minimum photon collection efficiency state detection error is because of the high  $P_{1/2}$  state to  $S_{1/2}$  state branching fraction of 99.5% [21] and the nonsequential ordering of the four hyperfine levels in the  $D_{3/2}$  state, which results in a larger detuning than sequential ordering.

#### IV. TWO LASER CLOCK OPERATION

A three-level clock may also enable clock operation with only two lasers addressing two electronic transitions. The ion could be laser cooled by strongly driving the  $S_{1/2} \rightarrow D_{3/2}$  electric quadrupole transition and repumping with the  $D_{3/2} \rightarrow P_{1/2}$  transition. Laser cooling has been achieved on the similar  $S_{1/2} \rightarrow D_{5/2}$  electric quadrupole transition in  $^{40}\text{Ca}^+$  [45]. For a three-level clock cooling on the  $S_{1/2} \rightarrow D_{5/2}$  transition drops the

TABLE II. Candidate alkaline-earth-like isotopes and their relevant atomic properties are given, including the half-life, nuclear spin  $I$ , magic rf trap drive frequency  $\Omega_{\text{rf}}$ , and hyperfine splittings,  $\text{HF}_n$ , of the  $S_{1/2}$  and  $P_{1/2}$  electronic states. The evaluated  $|S_{1/2}, F, m = 0\rangle \rightarrow |D_{3/2}, F', m = 0\rangle$  clock transition and quadratic Zeeman (QZ) shift at zero magnetic field are shown.  $\epsilon_{\text{bd}}$  ( $\epsilon_{\text{db}}$ ) are probability for bright-to-dark (dark-to-bright) errors due to off-resonant scattering.

Species	Half-life	$I$	$\Omega_{\text{rf}}$ (MHz)	$\text{HF}_S$ (GHz)	$\text{HF}_P$ (GHz)	Clock $F \rightarrow F'$	QZ (Hz/G <sup>2</sup> )	$\epsilon_{\text{bd}}$	$\epsilon_{\text{db}}$
<sup>43</sup> Ca <sup>+</sup>	stable	7/2	23.0	3.2 [34]	0.6 [35]	3 $\rightarrow$ 5	-3732	8.2e-6	9.6e-3
<sup>87</sup> Sr <sup>+</sup>	stable	9/2	15.0	5.0 [36]	0.9 [37]	4 $\rightarrow$ 6	-3400	2.7e-6	1.0e-4
<sup>133</sup> Ba <sup>+</sup>	10.5 y	1/2	3.4	9.9 [38]	1.8 [38]	0 $\rightarrow$ 2	-532	8.6e-6	2.9e-7
<sup>135</sup> Ba <sup>+</sup>	stable	3/2	3.3	7.2 [39]	1.3 [40]	1 $\rightarrow$ 3	1321	5.1e-6	8.7e-5
<sup>137</sup> Ba <sup>+</sup>	stable	3/2	3.3	8.0 [39]	1.5 [40]	1 $\rightarrow$ 3	1162	4.0e-6	6.8e-5
<sup>171</sup> Yb <sup>+</sup>	stable	1/2	7.7	12.6 [41]	2.1 [41]	0 $\rightarrow$ 2	519	7.2e-6	2.9e-7
<sup>173</sup> Yb <sup>+</sup>	stable	5/2	7.6	10.5 [41]	1.7 [41]	2 $\rightarrow$ 1	1526	2.4e-8	4.7e-8
<sup>223</sup> Ra <sup>+</sup>	11.4 d	3/2	6.1	6.8 [42]	1.3 [42]	1 $\rightarrow$ 3	1205	1.8e-6	9.6e-6
<sup>225</sup> Ra <sup>+</sup>	14.9 d	1/2	6.0	27.7 [42]	5.4 [42]	0 $\rightarrow$ 2	-321	8.9e-7	4.3e-8

requirement to drive the  $S_{1/2} \rightarrow P_{1/2}$  transition. For <sup>225</sup>Ra<sup>+</sup> the clock would only need 828 nm and 1079 nm lasers, see Fig. 4. To perform Doppler cooling the  $|S_{1/2}, F = 0\rangle \rightarrow |D_{3/2}, F = 2\rangle$  and  $|S_{1/2}, F = 1\rangle \rightarrow |D_{3/2}, F = 1\rangle$  transitions are driven while driving the  $|D_{3/2}, F = 2\rangle \rightarrow |P_{1/2}, F = 1\rangle$  and  $|D_{3/2}, F = 1\rangle \rightarrow |P_{1/2}, F = 1\rangle$  transitions to repump population. The population is then prepared in the  $|S_{1/2}, F = 0, m = 0\rangle$  state by turning off the light driving the  $|S_{1/2}, F = 0\rangle \rightarrow |D_{3/2}, F = 2\rangle$  transition. For clock interrogation, the  $|S_{1/2}, F = 0, m = 0\rangle \rightarrow |D_{3/2}, F = 2, m = 0\rangle$  transition is driven, followed by a  $|D_{3/2}, F = 2, m = 0\rangle \rightarrow |D_{3/2}, F = 1, m = 0\rangle$  microwave  $\pi$ -pulse at 1.3 GHz which populates a bright state if the clock transition was driven. The  $|S_{1/2}, F = 1\rangle \rightarrow |D_{3/2}, F = 1\rangle$  and  $|D_{3/2}, F = 1\rangle \rightarrow |P_{1/2}, F = 0\rangle$  transitions are then driven for state detection. More power would be needed at 828 nm for laser cooling compared to the three laser schemes described in Sec. II, but the trade-off in power could be enabling for integrated photonics as the only required wavelengths are now in the IR.

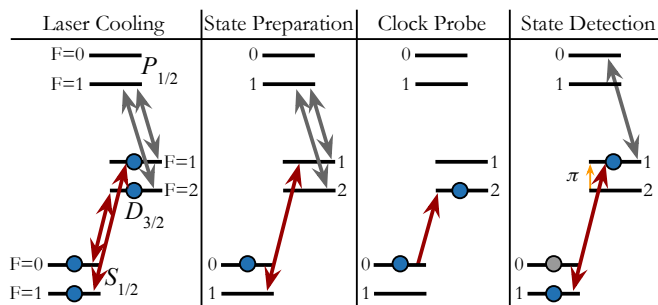


FIG. 4. Clock measurement sequences for a two-laser <sup>225</sup>Ra<sup>+</sup> ion optical clock based on the  $S_{1/2} \rightarrow D_{3/2}$  transition (red), which is also used for Doppler cooling. Arrows represent transitions between hyperfine levels, blue circles represent populated hyperfine levels, and gray circles represent the dark state during state detection. The  $D_{3/2} \rightarrow P_{1/2}$  repump transition (gray) and  $|D_{3/2}, F = 2, m = 0\rangle \rightarrow |D_{3/2}, F = 1, m = 0\rangle$  microwave transition (yellow) are shown.

## V. CONCLUSION

We have proposed three-level clocks with alkaline-earth-like ions with non-zero nuclear spin based on the  $S_{1/2} \rightarrow D_{3/2}$  transition. We show that heavy species with large hyperfine splittings, including <sup>133</sup>Ba<sup>+</sup>, <sup>171</sup>Yb<sup>+</sup>, <sup>173</sup>Yb<sup>+</sup>, <sup>223</sup>Ra<sup>+</sup>, and <sup>225</sup>Ra<sup>+</sup>, are promising for realizing such clocks. We highlight <sup>225</sup>Ra<sup>+</sup> as a candidate system for a three-level transportable clock due to its low state detection infidelity, ability to achieve low total systematic uncertainty, and suitability for integrated photonics [44]. Optical losses in integrated photonics generally decrease the farther the light is from the UV [46, 47], which makes clock species such as Ra<sup>+</sup> [44], whose shortest wavelength is at 468 nm, see Fig. 1, promising for integrated photonics. The radium ion clock  $\lambda = 828$  nm and repump  $\lambda = 1079$  nm transitions could also be frequency summed to generate the  $\lambda = 468$  nm Doppler cooling light, eliminating the need for a blue laser.

Among the alkaline-earth elements, the radium ion has the lowest sensitivity to blackbody radiation, and is promising for reaching total systematic uncertainty at the low  $10^{-18}$  level [44, 48]. Similar to the other alkaline-earth-like ions, the radium ion's  $S_{1/2} \rightarrow D_{3/2}$  clock transition has a negative differential scalar polarizability clock transition, see Table I. This enables operation at a magic rf trap drive frequency, see Table III, such that the micromotion induced-scalar Stark shift and the second-order Doppler shift cancel [49]. For <sup>225</sup>Ra<sup>+</sup>, the quadratic Zeeman shift coefficient at zero field is smaller than that of the <sup>171</sup>Yb<sup>+</sup> ion, see Table II. In a clock frequency comparison with a protocol proposed here Ra<sup>+</sup> could help improve the constraints on  $\dot{\alpha}/\alpha$  [50]. For Ra<sup>+</sup>, the sensitivity  $K$  to the time variation of the fine structure constant  $\dot{\alpha}/\alpha$  of the  $S_{1/2} \rightarrow D_{3/2}$  clock transition  $K_{3/2} = 3.03$  is higher than the  $S_{1/2} \rightarrow D_{5/2}$  transition  $K_{5/2} = 2.78$ , which is the largest positive  $K$  among demonstrated optical clocks [51]. This increase in sensitivity also comes with an improved stability because of the  $D_{3/2}$  state lifetime 638(10) ms that is more than a factor of two longer compared to the  $D_{5/2}$  state lifetime

303(4) ms [24].

We thank Sam Brewer and Shimon Kolkowitz for feedback on the manuscript, and Dave Leibbrandt for helpful discussions and pointing out reference [45]. This research

was performed under the sponsorship of ONR Grant No. N00014-21-1-2597, DoE grant DE-SC0022034, and NSF grant 2146555.

- 
- [1] M. Takamoto, I. Ushijima, N. Ohmae, T. Yahagi, K. Kokado, H. Shinkai, and H. Katori, *Nat. Photonics* **14**, 411 (2020).
- [2] A. Derevianko and M. Pospelov, *Nat. Phys.* **10**, 933 (2014).
- [3] A. D. Ludlow, M. M. Boyd, J. Ye, E. Peik, and P. O. Schmidt, *Rev. Mod. Phys.* **87**, 637 (2015).
- [4] E. A. Burt, J. D. Prestage, R. L. Tjoelker, D. G. Enzer, D. Kuang, D. W. Murphy, D. E. Robison, J. M. Seubert, R. T. Wang, and T. A. Ely, *Nature* **595**, 43 (2021).
- [5] K. Bely *et al.* (Boulder Atomic Clock Optical Network (BACON) Collaboration), *Nature (London)* **591**, 564 (2021).
- [6] Y. Huang, H. Zhang, B. Zhang, Y. Hao, H. Guan, M. Zeng, Q. Chen, Y. Lin, Y. Wang, S. Cao, K. Liang, F. Fang, Z. Fang, T. Li, and K. Gao, *PRA* **102**, 050802 (2020).
- [7] W. Loh, J. Stuart, D. Reens, C. D. Bruzewicz, D. Braje, J. Chiaverini, P. W. Juodawlakis, J. M. Sage, and R. McConnell, *Nature* **588**, 244 (2020).
- [8] A. A. Madej, J. E. Bernard, P. Dubé, L. Marmet, and R. S. Windeler, *Phys. Rev. A* **70**, 012507 (2004).
- [9] M. Chwalla, J. Benhelm, K. Kim, G. Kirchmair, T. Monz, M. Riebe, P. Schindler, A. S. Villar, W. Hänsel, C. F. Roos, R. Blatt, M. Abgrall, G. Santarelli, G. D. Rovera, and P. Laurent, *PRL* **102**, 023002 (2009).
- [10] J. Jin and D. A. Church, *Phys. Rev. Lett.* **70**, 3213 (1993).
- [11] M. Ramm, T. Pruttivarasin, M. Kokish, I. Talukdar, and H. Häffner, *Phys. Rev. Lett.* **111**, 023004 (2013).
- [12] M. S. Safronova and U. I. Safronova, *Phys. Rev. A* **83**, 012503 (2011).
- [13] A. Kreuter, C. Becher, G. P. T. Lancaster, A. B. Mundt, C. Russo, H. Häffner, C. Roos, W. Hänsel, F. Schmidt-Kaler, R. Blatt, and M. S. Safronova, *PRA* **71**, 032504 (2005).
- [14] C. Guet and W. R. Johnson, *Phys. Rev. A* **44**, 1531 (1991).
- [15] H. Zhang, M. Gutierrez, G. H. Low, R. Rines, J. Stuart, T. Wu, and I. Chuang, *New Journal of Physics* **18**, 123021 (2016).
- [16] B. K. Sahoo, R. G. E. Timmermans, B. P. Das, and D. Mukherjee, *PRA* **80**, 062506 (2009).
- [17] S. Mannervik, J. Lidberg, L.-O. Norlin, P. Royen, A. Schmitt, W. Shi, and X. Tordoir, *Phys. Rev. Lett.* **83**, 698 (1999).
- [18] K. J. Arnold, S. R. Chanu, R. Kaewuam, T. R. Tan, L. Yeo, Z. Zhang, M. S. Safronova, and M. D. Barrett, *PRA* **100**, 032503 (2019).
- [19] N. Yu, W. Nagourney, and H. Dehmelt, *Phys. Rev. Lett.* **78**, 4898 (1997).
- [20] S. Olmschenk, D. Hayes, D. N. Matsukevich, P. Maunz, D. L. Moehring, K. C. Younge, and C. Monroe, *PRA* **80**, 022502 (2009).
- [21] S. Olmschenk, K. C. Younge, D. L. Moehring, D. N. Matsukevich, P. Maunz, and C. Monroe, *PRA* **76**, 052314 (2007).
- [22] T. Schneider, E. Peik, and C. Tamm, *PRL* **94**, 230801 (2005).
- [23] C. Gerz, J. Roths, F. Vedel, and G. Werth, *Zeitschrift für Physik D Atoms, Molecules and Clusters* **8**, 235 (1988).
- [24] R. Pal, D. Jiang, M. S. Safronova, and U. I. Safronova, *Phys. Rev. A* **79**, 062505 (2009).
- [25] M. Fan, C. A. Holliman, A. L. Wang, and A. M. Jayich, *PRL* **122**, 223001 (2019).
- [26] J. Stenger, C. Tamm, N. Haverkamp, S. Weyers, and H. R. Telle, *Opt. Lett.* **26**, 1589 (2001).
- [27] R. J. Rafac, B. C. Young, J. A. Beall, W. M. Itano, D. J. Wineland, and J. C. Bergquist, *Phys. Rev. Lett.* **85**, 2462 (2000).
- [28] G. P. Barwood, K. Gao, P. Gill, G. Huang, and H. A. Klein, *PRA* **67**, 013402 (2003).
- [29] J. Benhelm, G. Kirchmair, U. Rapol, T. Körber, C. F. Roos, and R. Blatt, *PRA* **75**, 032506 (2007).
- [30] M. R. Dietrich, N. Kurz, T. Noel, G. Shu, and B. B. Blinov, *PRA* **81**, 052328 (2010).
- [31] T. Schneider, *Optical Frequency Standard with a Single  $^{171}\text{Yb}^+$  Ion*, Ph.D. thesis, University of Hannover (2005).
- [32] V. Letchumanan, P. Gill, E. Riis, and A. G. Sinclair, *PRA* **70**, 033419 (2004).
- [33] F. A. An, A. Ransford, A. Schaffer, L. R. Sletten, J. Gaebler, J. Hostetter, and G. Vittorini, *PRL* **129**, 130501 (2022).
- [34] F. Arbes, M. Benzing, T. Gudjons, F. Kurth, and G. Werth, *Zeitschrift für Physik D Atoms, Molecules and Clusters* **31**, 27 (1994).
- [35] W. Nörtershäuser, K. Blaum, K. Icker, P. Müller, A. Schmitt, K. Wendt, and B. Wiche, *The European Physical Journal D - Atomic, Molecular, Optical and Plasma Physics* **2**, 33 (1998).
- [36] H. Sunaoshi, Y. Fukushima, M. Furukawa, M. Yamauchi, S. Hayashibe, T. Shinozuka, M. Fujioka, I. Satoh, M. Wada, and S. Matsuki, *Hyperfine Interactions* **78**, 241 (1993).
- [37] U. I. Safronova, *PRA* **82**, 022504 (2010).
- [38] D. Hucul, J. E. Christensen, E. R. Hudson, and W. C. Campbell, *Phys. Rev. Lett.* **119**, 100501 (2017).
- [39] W. Becker, R. Blatt, and G. Werth, *Journal de Physique Colloques* **42**, C8 (1981).
- [40] M. Van Hove, G. Borghs, P. De Bisschop, and R. E. Silverans, *Zeitschrift für Physik A Atoms and Nuclei* **321**, 215 (1985).
- [41] A.-M. Mårtensson-Pendrill, D. S. Gough, and P. Hanaford, *PRA* **49**, 3351 (1994).
- [42] W. Neu, R. Neugart, E. W. Otten, G. Passler, K. Wendt, B. Fricke, E. Arnold, H. J. Kluge, and G. Ulm, *Zeitschrift für Physik D Atoms, Molecules and Clusters* **11**, 105 (1989).
- [43] B. K. Sahoo, B. P. Das, R. K. Chaudhuri, D. Mukherjee, R. G. E. Timmermans, and K. Jungmann, *Phys. Rev. A*

- 76**, 040504 (2007).
- [44] C. A. Holliman, M. Fan, A. Contractor, S. M. Brewer, and A. M. Jayich, PRL **128**, 033202 (2022).
- [45] R. J. Hendricks, J. L. Sørensen, C. Champenois, M. Knoop, and M. Drewsen, PRA **77**, 021401 (2008).
- [46] X. Liu, A. W. Bruch, Z. Gong, J. Lu, J. B. Surya, L. Zhang, J. Wang, J. Yan, and H. X. Tang, Optica **5**, 1279 (2018).
- [47] G. N. West, W. Loh, D. Kharas, C. Sorace-Agaskar, K. K. Mehta, J. Sage, J. Chiaverini, and R. J. Ram, APL Photonics **4**, 026101 (2019).
- [48] O. O. Versolato, L. W. Wansbeek, K. Jungmann, R. G. E. Timmermans, L. Willmann, and H. W. Wilschut, PRA **83**, 043829 (2011).
- [49] P. Dubé, A. A. Madej, M. Tibbo, and J. E. Bernard, PRL **112**, 173002 (2014).
- [50] R. Lange, N. Huntemann, J. M. Rahm, C. Sanner, H. Shao, B. Lipphardt, C. Tamm, S. Weyers, and E. Peik, PRL **126**, 011102 (2021).
- [51] V. V. Flambaum and V. A. Dzuba, Can. J. Phys. **87**, 25 (2009).